

Spontaneously ordered motion of self-propelled particles

András Czirók^{1,2}, H. Eugene Stanley¹ and Tamás Vicsek²

¹ Center for Polymer Studies and Department of Physics, Boston University, Boston, MA 02215

² Department of Atomic Physics, Eötvös University, Budapest, Puskin u. 5-7, 1088 Hungary

We study a biologically inspired, inherently non-equilibrium model consisting of self-propelled particles. In the model, particles move on a plane with a velocity of constant magnitude; they locally interact with their neighbors by choosing at each time step a velocity direction equal to the average direction of their neighbors. Thus, in the limit of vanishing velocities the model becomes analogous to a Monte-Carlo realization of the classical XY ferromagnet. We show by large-scale numerical simulations that, unlike in the equilibrium XY model, a long-range ordered phase characterized by non-vanishing net flow ϕ emerges in this system in a phase space domain bordered by a critical line along which the fluctuations of the order parameter diverge. The corresponding phase diagram as a function of two parameters, the amplitude of noise η and the average density of the particles ρ is calculated and is found to have the form $\eta_c(\rho) \sim \rho^{1/2}$. We also find that ϕ scales as a function of the external bias h (field or “wind”) according to a power law $\phi \sim h^{0.9}$. In the ordered phase the system shows long-range correlated fluctuations and $1/f$ noise.

I. INTRODUCTION

Recently there has been an increasing interest in the studies of far-from-equilibrium systems typical in our natural and social environment. Concepts originated from the physics of phase transitions in equilibrium systems [1] such as collective behavior, scale invariance and renormalization have been shown to be useful in the understanding of various non-equilibrium systems as well. Simple algorithmic models have been helpful in the extraction of the basic properties of various far-from-equilibrium phenomena, like diffusion limited growth [2], self-organized criticality [3] or surface roughening [4]. Motion and related transport phenomena represent a further characteristic aspect of non-equilibrium processes. Indeed, the transport in various driven systems, such as traffic models [5], molecular motors [6] and other self-propelled systems [7–12] have been the subject of recent studies.

Self-propulsion is an essential feature of most living systems. Moreover, the motion of the organisms is usually controlled not only by some external fields, but also by interactions with other organisms in their neighborhood. In Ref. [7], a simple model was introduced capturing these features with a view toward modeling the

collective motion of large groups of organisms [13–16] such as schools of fish, herds of quadrupeds, flocks of birds, or groups of migrating bacteria [17–21]. The aim of this paper is to further investigate the various interesting phenomena exhibited by this novel non-equilibrium model.

The model consists of particles moving on a plane and characterized by their (off-lattice) location \vec{x}_i and velocity \vec{v}_i pointing in the direction $\vartheta_i = \Theta(\vec{v}_i)$, where the function Θ gives the angle between its argument vector and a selected direction (e.g., horizontal coordinate axis). The magnitude of the velocity is fixed to v_0 to account for the *self-propelled* nature of the particles. A simple local interaction is defined in the model: at each time step a given particle assumes the average direction of motion of the particles in its local neighborhood $S(i)$ with some uncertainty, as described by

$$\vartheta_i(t + \Delta t) = \langle \vartheta \rangle_{S(i)} + \xi, \quad (1)$$

where the noise ξ is a random variable with a uniform distribution in the interval $[-\eta/2, \eta/2]$ and the local average direction of motion $\langle \vartheta \rangle_{S(i)}$ is defined as

$$\langle \vartheta \rangle_{S(i)} = \Theta \left(\sum_{\vec{x}_j \in S(i)} \vec{v}_j \right). \quad (2)$$

The local surrounding of the i th particle $S(i)$ will be specified in Sec. II. The locations of the particles are updated in each time step as

$$\vec{x}_i(t + \Delta t) = \vec{x}_i(t) + \vec{v}_i(t)\Delta t. \quad (3)$$

This model is a transport related, non-equilibrium analog of the *ferromagnetic* models, with the important difference that it is inherently *dynamic*: the elementary event is the motion of a particle at each time step and a change in the direction of motion. The analogy is as follows: the Hamiltonian tending to align the spins in the same direction in the case of equilibrium ferromagnets is replaced by the rule of aligning the direction of motion of particles. The amplitude of the random perturbations is in analogy with the temperature [7]. Indeed, if $v_0 = 0$, the model is similar to the Monte-Carlo simulations of diluted XY ferromagnets [22].

The reported long-range order in the above [7] and the closely related models [10,11] is surprising, because in the case of equilibrium systems possessing continuous rotational symmetry the ordered phase is destroyed at finite temperatures [23]. A recent dynamic renormalization group treatment of the problem [9] by Tu and Toner

has also led to the conclusion of the existence of an ordered phase in two dimensions. Thus, the question of how the ordered phase emerges due to the non-equilibrium nature of the model is of considerable theoretical interest as well. In Section II we study the kinetic phase transition leading to the symmetry-broken state, which is characterized in Section III. In Section IV, we investigate the effect of an external field applied to the system.

II. KINETIC PHASE TRANSITION

We studied the behavior of the model defined through Eqs. (1)-(3) by performing large-scale Monte-Carlo simulations as a function of two control parameters: the density of particles ϱ and amplitude of the noise η . We applied random initial conditions and periodic boundary conditions. The calculations were performed on a *Connection Machine 5* parallel computer, with typically $N = 10^4 - 10^5$ particles.

The interaction range of $S(i)$ was defined in two different ways: (i) as a circle of radius R , or (ii) by considering a square lattice on the plane built up from lattice cells of length R , and assuming that a given particle interacts with all the particles located in the same lattice cell and in the eight neighboring cells (see Fig. 1). The existence of the long-range order, and the critical exponents, turned out to be *robust* against changing these details [(i) or (ii)] of the interaction. Here we present results obtained by definition (ii), as this latter choice of $S(i)$ increases the speed of the simulations by a considerable amount.

A natural dimensionless parameter is $C \equiv v_0 \Delta t / R$, and the behavior of the model on v_0 , Δt and R depends only through their combination given in this expression for C . Thus, we can work with $\Delta t = 1$ and $R = 1$. The results presented in the following were obtained with $v_0 = 0.1$, the role of this velocity is discussed in Sec. V.

For the statistical characterization of the model, a well-suited order parameter is the magnitude of the average momentum of the system:

$$\phi \equiv \frac{1}{N} \left| \sum_j \vec{v}_j \right|. \quad (4)$$

This measure of the net flow is non-zero in the ordered phase, and vanishes (for an infinite system) in the disordered phase.

We start the simulations from a disordered system (random positions and orientations), thus $\phi(t=0) \approx 0$. After some relaxation time a steady state emerges indicated, e.g., by the convergence of the cumulative average $(1/\tau) \int_0^\tau \phi(t) dt$. Here we focus on the statistical properties of the steady state only, and do not deal with the entire relaxation process. In the vicinity of the critical regime to reach the stationary behavior takes more than 10^4 Monte-Carlo steps for a typical simulation with 10^5

particles in a 100×100 system. In such cases we run the simulations for $\approx 10^5$ time steps, which takes about 4 hours CPU time on the *CM5*.

The stationary values of ϕ that we obtained as a time average are plotted in Fig. 2a vs η for $\varrho = 2$ and various system sizes. In agreement with Ref. [7], for weak noise the model displays long-range ordered motion (up to the actual system size L), that disappears in a continuous manner by increasing η .

As $L \rightarrow \infty$, the numerical results indicate the presence of a kinetic phase transition described by

$$\phi(\eta) \sim \begin{cases} \left(\frac{\eta_c(\varrho, L) - \eta}{\eta_c(\varrho, L)} \right)^\beta & \text{for } \eta < \eta_c(\varrho, L) \\ 0 & \text{for } \eta > \eta_c(\varrho, L) \end{cases}, \quad (5)$$

where $\eta_c(\varrho, L)$ is the critical noise amplitude that separates the ordered and disordered phases. For a given set of $\phi(\eta)$, the exponent β and $\eta_c(\varrho, L)$ is determined by selecting the values providing the best fit to the *Ansatz* (5), i.e., yielding the maximal scaling regime. The numerical results are consistent with (5), since the scaling regime is increased for larger N (Fig. 2b) and the estimated values of $\eta_c(\varrho, L)$ converge to a non-zero $\eta_c(\varrho, \infty)$ value as

$$\eta_c(\varrho, L) - \eta_c(\varrho, \infty) \sim N^{-\zeta}, \quad (6)$$

where ζ is approximately equal to 0.25 (Fig. 2c). This calculation yields (for $\varrho = 2$) $\beta = 0.42 \pm 0.03$, which is definitely different from the the mean-field value $1/2$, and consistent with the value reported in [7] obtained for smaller systems using definition (i) for $S(i)$.

Next we discuss the role of density. In Fig. 3a, $\phi(\eta)$ is plotted for $L = 100$ and various values of ϱ . One can observe that the long-range ordered phase is present for any ϱ , but for a fixed value of η , ϕ vanishes with decreasing ϱ . These $\phi(\eta)$ functions parameterized by various ϱ collapse to a “universal” function $\tilde{\phi}(x)$ by rescaling η with $\eta_c(\varrho)$,

$$\phi(\eta, \varrho) = \tilde{\phi}(\eta/\eta_c(\varrho)), \quad (7)$$

where $\tilde{\phi}(x) \sim (1-x)^\beta$ for $x < 1$, and $\tilde{\phi}(x) \approx 0$ for $x > 1$, and $\eta_c(\varrho)$ is determined as the value which minimizes

$$\Delta(z) = \left[\int_0^A dx \left(\phi(xz, \varrho) - \tilde{\phi}(x) \right) \right]^2. \quad (8)$$

Here the $A < 1$ cutoff is chosen to exclude the noisy and rounded (due to finite-size effects) region around η_c . In our calculations we used the value $A = 0.9$, and we determined $\tilde{\phi}(x)$ in a self-consistent manner by averaging over the already rescaled $\phi(\eta/\eta_c(\varrho))$ functions. We show the result of the data collapse in Fig. 3b.

This procedure (together with the finite-size analysis for a given ϱ) also yields the position of the “critical line” $\eta_c(\varrho)$ in the $\eta - \varrho$ parameter space. According to our numerical results,

$$\eta_c(\varrho) \sim \varrho^\kappa \quad (9)$$

holds with $\kappa = 0.45 \pm 0.05$ (see Fig. 3c). Apart from the numerical uncertainties, $\kappa = 1/2$, in agreement with recent theoretical results [24].

The critical line (9) is qualitatively different from that of the diluted ferromagnets, since here the critical density at $\eta \rightarrow 0$ (corresponding to the percolation threshold for diluted ferromagnets, see, e.g., [22]) is vanishing,

$$\lim_{\eta \rightarrow 0} \varrho_c(\eta) = 0. \quad (10)$$

To see this, let us imagine a system of size L consisting of two particles only. Due to the finite size of $S(i)$, for almost all initial conditions the trajectories of these particles will get close enough to each other to establish interaction. As the noise is negligible in (1), the cluster formed by the particles will not break apart, resulting in $\phi \approx 1$ for any finite ϱ as $\eta \rightarrow 0$.

The behavior of the model in the $\varrho \rightarrow \infty$ limit is still not clear. By definition $\eta < 2\pi$ holds, so (9) obviously cannot describe the system in this limit. Thus $\eta_c(\varrho)$ either approaches 2π or a non-trivial $\eta_c(\infty) < 2\pi$ value.

Finally we note that Eq.(7) also implies that the exponent β' , defined as $\phi \sim (\varrho - \varrho_c)^{\beta'}$ for $\varrho > \varrho_c$ (see Ref. [7]), must be equal to β , since

$$\phi(\eta, \varrho_c(\eta) + \epsilon) = \tilde{\phi} \left(\frac{\eta}{\eta_c[\varrho_c(\eta) + \epsilon]} \right) \approx \tilde{\phi} \left(1 - \frac{1}{\eta} \frac{\partial \eta_c}{\partial \varrho} \epsilon \right) \sim \epsilon^\beta, \quad (11)$$

where $\eta_c(\varrho)$ denotes the inverse function of $\varrho_c(\eta)$ as $\eta \equiv \eta_c[\varrho_c(\eta)]$. Indeed, the results of the simulations performed with $\eta = \text{const}$ and various L and ρ yield $\beta' = 0.4 \pm 0.05$, which is consistent with $\beta = \beta'$. In this case the larger uncertainty is due to the increased noise at low densities.

III. FLUCTUATIONS

As a further analogy with equilibrium phase transitions, we note that the fluctuations of the order parameter also increase on approaching the critical line. To study this, we calculate for various control parameters the standard deviation of the total momentum, defined as $\sigma^2 \equiv \langle \phi^2 \rangle - \langle \phi \rangle^2$, where the averages are taken over the stationary data set obtained from the simulations. In Fig. 4a we plot σ vs the rescaled noise amplitude $x \equiv \eta/\eta_c(\varrho)$ for various densities and $L = 100$. The tails of the curves are symmetric, and decay as power-laws with an exponent γ close to 2 (see Fig. 4b)

$$\sigma(x) \sim |1 - x|^{-\gamma}. \quad (12)$$

In Sec. IV we compare this result to direct susceptibility measurements, when an external field is also applied.

We studied the time correlations of the fluctuations by calculating the expected value of the rms deviation in a time interval Δt

$$w_\phi^2(\Delta t) = \langle \langle \phi^2 \rangle_{\Delta t} - \langle \phi \rangle_{\Delta t}^2 \rangle, \quad (13)$$

where the internal and external brackets denote averages calculated over a time interval $[t, t + \Delta t]$ and the entire stationary data set, respectively. A close relation between $w_\phi(\Delta t)$ and the power-spectrum $S_\phi(\omega)$ of the order parameter $\phi(t)$ can be derived from the self-affine properties of the signal [25]: $w_\phi(\Delta t) \sim (\Delta t)^\alpha$ is equivalent to $S_\phi(\omega) \sim \omega^{-\lambda}$, and for the exponents $\lambda = 1 + 2\alpha$ holds (for $3 > \lambda > 1$).

The numerically obtained results (Fig. 5a) show that at the critical line the fluctuations of the order parameter are characterized by the correlation exponent $\alpha = 0.6 \pm 0.05$ up to a characteristic correlation time τ . This behavior means that in the steady state the ‘condensation’ and ‘evaporation’ processes (when particles join or leave the dominant cluster, respectively) are correlated [26]. For $t > \tau$ the system shows even stronger correlations, as in this regime $w_\phi(\Delta t) \sim \log \Delta t$ (see Fig. 5b). This behavior is probably related to the periodic boundary conditions, as τ is comparable to L/v_0 , the time needed for a particle to cross the entire system.

IV. EXTERNAL FIELD

The presence of the long-range correlated phase in two dimensions (i.e. the breakdown of the Mermin-Wagner theorem [23]) is a striking consequence of the non-equilibrium nature of the XY model. As the fluctuation-response theorem $kT\chi = N\sigma^2$ must hold for Hamiltonian systems only, it is interesting to check its applicability when the equation of motion cannot be derived from a Hamiltonian.

A natural way to introduce an external field in the model is by changing rule (2) for

$$\langle \vartheta \rangle_{S(i)} = \Theta \left(\sum_{\substack{j \\ \bar{x}_j \in S(i)}} \vec{v}_j + h\vec{e} \right). \quad (14)$$

where \vec{e} is an arbitrary unit vector and the parameter h controls the strength of the perturbation.

In the numerical studies we set the density of the particles to $\varrho = 2$, and study ϕ as a function of η and h . Typical results for systems of $L = 100$ are plotted in Fig. 6. The curves parameterized by various η intersect the $h = 0$ axis at the same values found in Sec. II, so for $h = 0$ the original model is recovered. In general, ϕ is increased for increasing h , and the results can be summarized by means of critical exponents δ , γ_* , γ'_* and susceptibility $\chi(\eta)$ defined in a manner similar to the case of classical magnets:

$$\chi(\eta) = \lim_{h \rightarrow 0} \frac{\phi(\eta, h) - \phi(\eta, h = 0)}{h}, \quad (15)$$

$$\phi \sim h^{1/\delta} \quad \text{for } \eta > \eta_c, \quad (16)$$

and

$$\chi(\eta) \sim \begin{cases} \left(\frac{\eta-\eta_c}{\eta_c}\right)^{-\gamma_*} & \text{for } \eta > \eta_c \\ \left(\frac{\eta_c-\eta}{\eta_c}\right)^{-\gamma'_*} & \text{for } \eta < \eta_c \end{cases} \quad (17)$$

We distinguish the critical exponents γ_* and γ'_* from the exponent γ defined by the singularity of $\sigma(\eta)$, since in this case $\gamma \neq \gamma_* \neq \gamma'_*$ (as will be demonstrated later).

To determine δ , we plot the obtained $\phi(\eta)$ curves on a double logarithmic plot (see Fig. 7a). We see that for large values of ϕ the system saturates ($\phi > \phi_{\text{sat}} \approx 0.1$), while for low values of ϕ the finite-size noise dominates ($\phi < \phi_{\text{noise}} \approx 0.03$, for $L = 100$). Thus, we expect that the relation

$$\phi(\eta, h) = \chi(\eta)h^{1/\delta} \quad (18)$$

holds for $\phi_* \in [\phi_{\text{noise}}, \phi_{\text{sat}}]$ only. As the boundaries of this interval do not depend on η until $\eta > \eta_c$, Eq. (18) can be verified by collapsing the rescaled $\phi_*(\eta, h)/\chi(\eta)$ data points onto a single power-law (Fig. 7b). Similarly to the determination of $\eta_c(\varrho)$, $\chi(\eta)$ and δ can be calculated in a self-consistent manner. This procedure yields $\delta = 1.1 \approx 1$ and $\chi(\eta)$ decaying with $\gamma_* \approx 4$. Note, that γ'_* cannot be obtained by this method as in the ordered phase $\phi > \phi_{\text{sat}}$.

To check the stability of these results, we also performed measurements on larger systems, where ϕ_{noise} is reduced. Indeed, the scaling regime for (18) increases and the exponent is consistent with our former estimate (see Fig. 7c)

We can also calculate $\chi(\eta)$ applying its definition (17) by sampling a series of $\chi(\eta)_i \equiv [\phi(\eta, h_i) - \phi(\eta, h'_i)]/(h_i - h'_i)$ for various $h_i, h'_i \ll 1$, and (as $\delta \approx 1$) assuming $\chi(\eta) = \langle \chi_i(\eta) \rangle_i$. The result is shown on Fig. 8. The $\eta > \eta_c$ tail is consistent with our former estimate from applying (18), while for $\eta < \eta_c$ $\chi(\eta)$ decays with $\gamma'_* \approx 1$.

V. CONCLUSIONS

We have demonstrated that this far-from-equilibrium system of self-propelled particles can be described using the framework of classical critical phenomena, but shows surprising new features when compared to the analogous equilibrium systems. The velocity v_0 provides a control parameter which switches between an equilibrium XY type model ($v_0 = 0$), and another universality class of dynamic, non-equilibrium models characterized by a non-vanishing value of v_0 .

Indeed, for $v_0 = 0$ we can observe Kosterlitz-Thouless vortices in the system, which turned out to be unstable for any nonzero v_0 we investigated: in Fig. 9 we plot snapshots of the system. These pictures demonstrate how the vortices disappear and give way to long-range order. We performed control simulations with various v_0 in the range $[0.01, 0.3]$, and the results presented seem to be robust against changing the value of v_0 in this range.

ACKNOWLEDGMENTS

We have benefited from discussions with E. Ben-Jacob, Z. Csahók, S. T. Harrington and H. Makse. This work was supported by the US-Hungarian Joint Fund Contract No. 352. and by the Hungarian Research Foundation grant No. T4439. A. Czirók is grateful to A.-L. Barabási for his kind hospitality during his visit at University of Notre Dame.

-
- [1] S.-K. Ma, *Statistical Mechanics* (World Scientific, Singapore, 1985); *Modern Theory of Critical Phenomena* (Benjamin, New York, 1976); H. E. Stanley, *Introduction to Phase Transitions and Critical Phenomena* (Oxford University Press, Oxford, 1971).
 - [2] T. A. Witten and L. M. Sander, Phys. Rev. Lett. **47**, 1400 (1981); T. Vicsek, *Fractal Growth Phenomena, Second Edition* (World Scientific, Singapore, 1992).
 - [3] P. Bak, C. Tang and K. Wiesenfeld, Phys. Rev. Lett. **59**, 381 (1987).
 - [4] A.-L. Barabási and H. E. Stanley, *Fractal Concepts in Surface Growth* (Cambridge University Press, Cambridge, 1995)
 - [5] See, e.g., K. Nagel and H. J. Herrmann, Physica A **199**, 254 (1993), and references therein
 - [6] M. O. Magnasco, Phys. Rev. Lett. **71**, 1477 (1993); A. Ajdari and J. Prost, C. R. Acad. Sci. Paris **315**, 1635 (1992); I. Derényi and T. Vicsek, Phys. Rev. Lett. **75**, 374 (1995).
 - [7] T. Vicsek, A. Czirók, E. Ben-Jacob, I. Cohen and O. Shochet, Phys. Rev. Lett. **75**, 1226 (1995).
 - [8] Z. Csahók and T. Vicsek, Phys. Rev. E **52**, 5297 (1995).
 - [9] J. Toner and Y. Tu, Phys. Rev. Lett. **75**, 4326 (1995).
 - [10] Y. L. Duparcmeur, H.J. Herrmann and J. P. Troadec, J. Phys. (France) I, **5**, 1119 (1995).
 - [11] J. Hemmingsson, J. Phys. **A 28**, 4245 (1995).
 - [12] E. V. Albano, Phys. Rev. Lett. **77**, 2129 (1996).
 - [13] C. W. Reynolds, Computer Graphics **21**, 25 (1987).
 - [14] D. P. O'Brien J. Exp. Mar. Biol. Ecol. **128**, 1 (1989).
 - [15] J. L. Deneubourg and S. Goss, Ethology, Ecology, Evolution **1**, 295 (1989).
 - [16] A. Huth and C. Wissel, in *Biological Motion*, eds. W. Alt and E. Hoffmann (Springer Verlag, Berlin, 1990).
 - [17] A. Czirók, E. Ben-Jacob, I. Cohen and T. Vicsek, "Formation of complex bacterial colonies via self generated vortices" (preprint)
 - [18] C. Allison and C. Hughes, Sci. Progress **75**, 403 (1991).
 - [19] E. Ben-Jacob, A. Tenenbaum, O. Shochet, O. Avidan, Physica A **202**, 1 (1994).
 - [20] E. Ben-Jacob, I. Cohen, O. Shochet, A. Tenenbaum, A. Czirók and T. Vicsek, Nature **368**, 46 (1994); *Fractals* **2**, 1 (1994).
 - [21] E. Ben-Jacob, I. Cohen, O. Shochet, A. Tenenbaum, A. Czirók and T. Vicsek, Phys. Rev. Lett. **75**, 2899 (1995).
 - [22] R. B. Stinchcombe in *Phase Transitions and Critical Phenomena*

nomena Vol. 7, eds. C. Domb and J. Lebowitz (Academic Press, New York, 1983).

- [23] N. D. Mermin and H. Wagner, *Phys. Rev. Lett.* **17**, 1133 (1966).
- [24] A.-L. Barabási and A. Czirók (preprint)
- [25] R. F. Voss, in *Scaling Phenomena in Disordered Systems*, edited by R. Pynn and A. Skjeltrop (Plenum Press, New York, 1985).
- [26] In the uncorrelated case the momentum of the dominant cluster would be the integral of an uncorrelated noise yielding $\alpha = 0.5$.

FIG. 1. Schematic illustration of the model. The particles move off-lattice on a plane and interact with other particles located in the local surrounding, which can be either a circle or 9 neighboring cells in an underlying lattice. We plot these interaction areas for particle A with a solid and dashed line, respectively.

FIG. 2. (a) The average momentum of the system in the steady state vs the noise amplitude η for $\varrho = 2$ and four different system sizes [(\diamond) $N = 800$, $L = 20$; (+) $N = 3200$, $L = 40$; (\square) $N = 20000$, $L = 100$ and (\times) $N = 10^5$, $L = 223$]. (b) The order present at small η disappears in a continuous manner reminiscent of second order phase transitions: $\phi \sim [(\eta_c(L) - \eta)/\eta_c(L)]^\beta \equiv (\Delta\eta/\eta_c)^\beta$, with $\beta = 0.42$, different from the mean-field value $1/2$ (solid line). (c) The estimated $\eta_c(L)$ values converge to a non-zero $\eta_c(\infty)$ limit as $L^{-1/2}$, indicating the presence of the ordered phase even as $N \rightarrow \infty$. The data represent time averages of long ($> 10^5$ MCS) simulations.

FIG. 3. (a) The average momentum of the system in the steady state vs η for $L = 100$ and three different densities [(\square) $\varrho = 4$, (\diamond) $\varrho = 2$ and (+) $\varrho = 0.5$]. (b) The $\phi(\eta)$ functions parameterized by various ϱ can be collapsed onto a single curve $\tilde{\phi}[\eta/\eta_c(\varrho)] \equiv \phi(\eta, \varrho)$. (c) The critical line in the $\eta - \varrho$ phase space is a power-law in the examined regime: $\eta_c(\varrho) \sim \varrho^\kappa$ with $\kappa \approx 0.45$ (solid line) for a system of size $L = 100$.

FIG. 4. (a) The rms deviation of the order parameter σ in the steady state, for $L = 100$, and two independent data sets (\diamond , +), each averaged over runs with $\varrho = 0.3, 0.6, 0.9, 1.2, 1.5$ and 2. (b) The divergence is symmetric and its tail decays as $\sigma(x) \sim |1 - x|^{-2}$ (solid line), where x denotes the rescaled noise amplitude $\eta/\eta_c(\varrho)$.

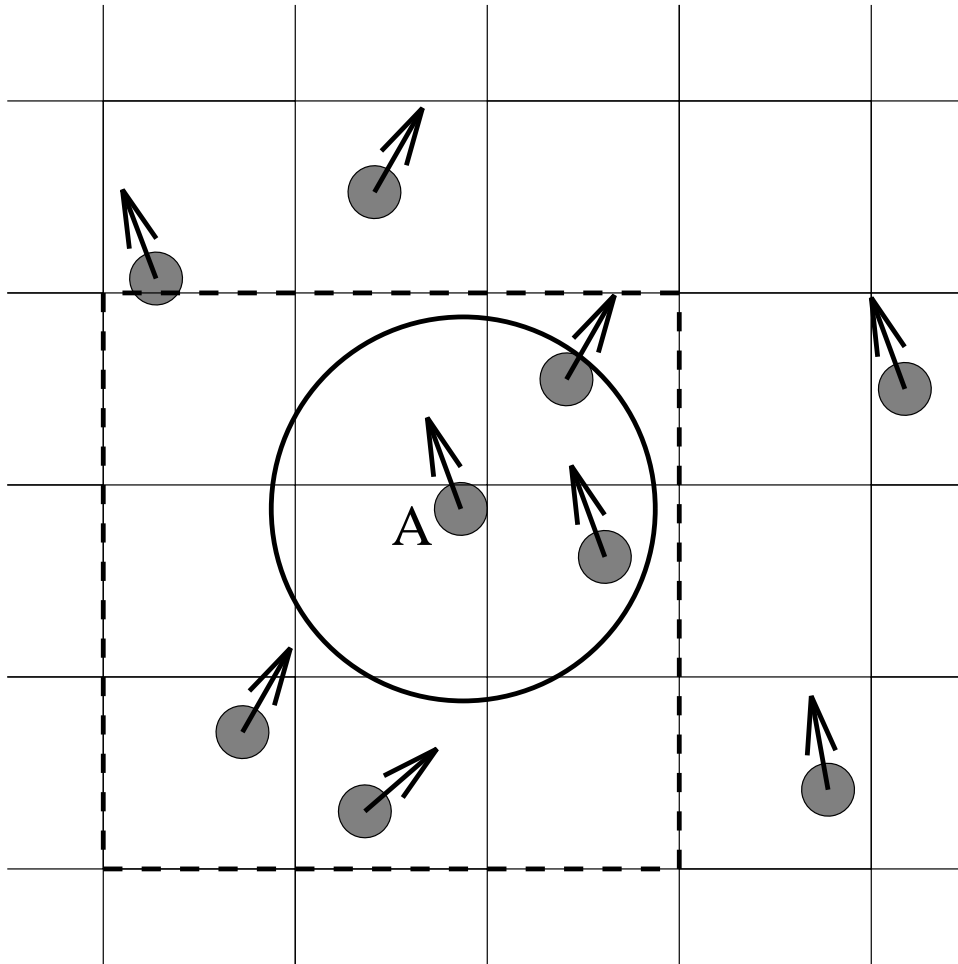
FIG. 5. The expected value of the standard deviation of the order parameter in a time interval of length Δt on double logarithmic (a) and log-linear (b) plots. For $\Delta t < \tau \approx L/v_0$ the system shows long-range correlations characterized by $w_\phi(\Delta t) \sim \Delta t^\alpha$ where $\alpha \approx 0.6$. For comparison, the dotted line shows the uncorrelated case ($\alpha = 1/2$). For $\Delta t > \tau$ the correlations are even stronger: $w_\phi(\Delta t) \sim \log(\Delta t)$. The data displayed is an average over two independent runs, each was performed at $\eta = 2.73$, $\varrho = 2$ and $N = 10^5$. The duration of the simulation was 70 000 Monte-Carlo steps.

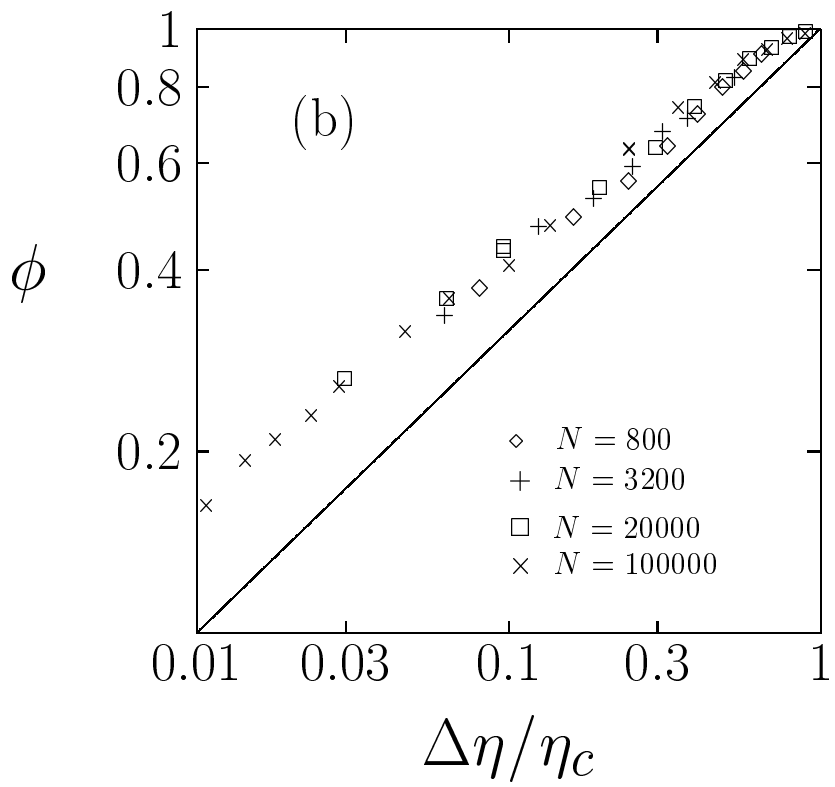
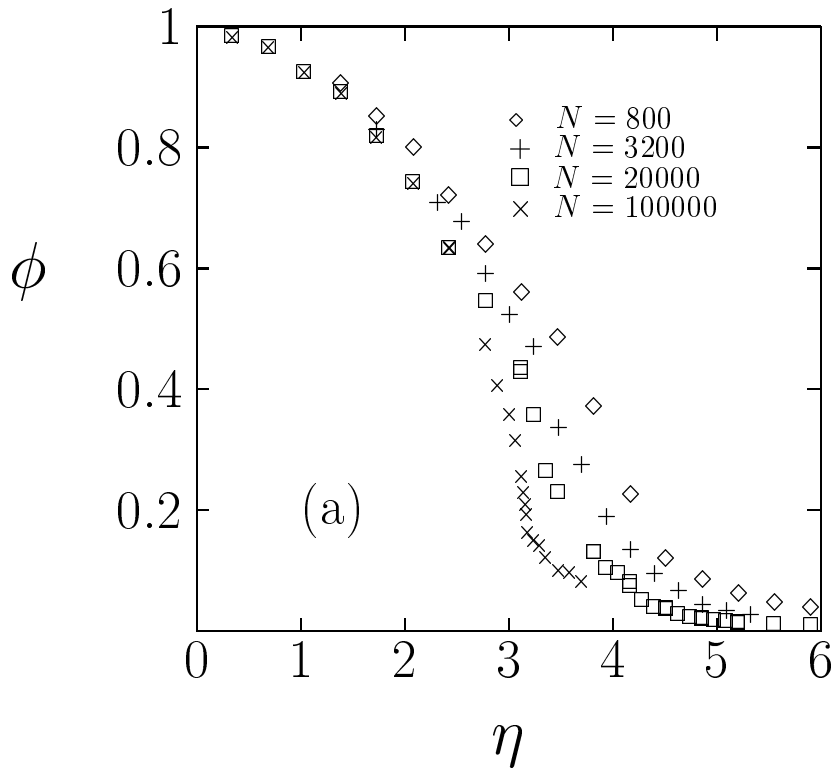
FIG. 6. ϕ vs the amplitude of the applied external field h , for $\varrho = 2$, $L = 100$ and $\eta = 0.3, 0.9, 1.5, 2.1, 2.7, 3.3, 3.5$ and 4.5 (from top to bottom).

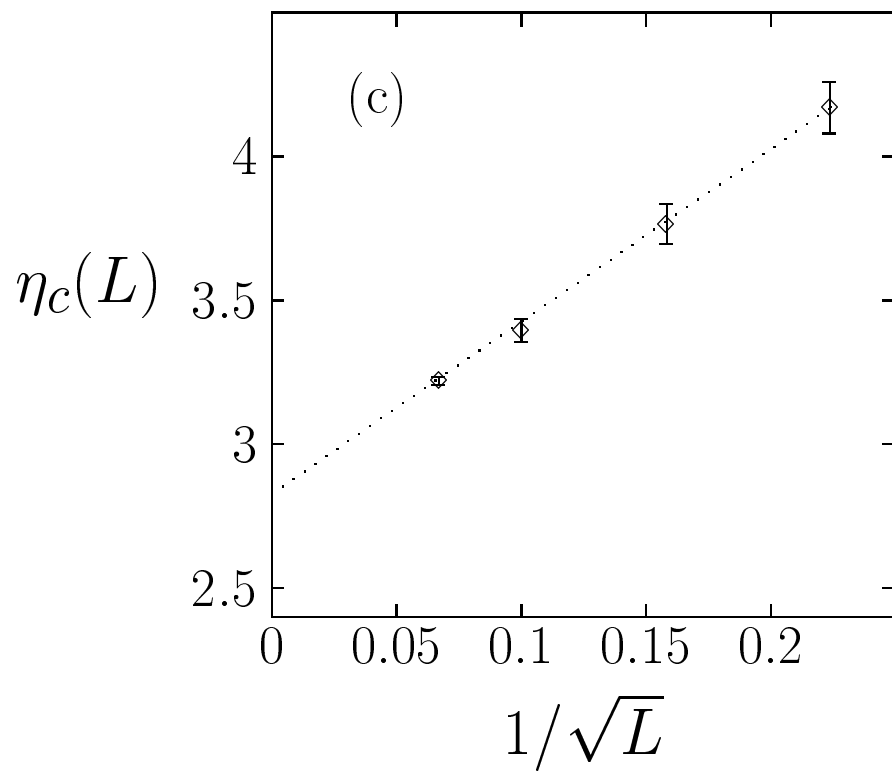
FIG. 7. (a) The $\phi(h)$ functions for $\varrho = 2$, $L = 100$ and $\eta = 3.9, 4.2, 4.5, 4.8, 5.2$ (from top to bottom) on a double-logarithmic plot. $\phi \sim h^{1/\delta}$ holds for a limited range of ϕ only, as for $\phi > 0.1$ the system saturates, and for $\phi < 0.02$ the finite-size noise dominates. (b) For $0.02 < \phi < 0.1$ the curves for various η can be collapsed onto a single power-law with an exponent $1/\delta \approx 0.9$. (c) For larger systems the finite-size noise is reduced and the scaling regime is enlarged, in agreement with the $\phi \sim h^{1/\delta}$ Ansatz [(\diamond) $\varrho = 2, L = 100$, $\eta = 4.2$; (+) $\varrho = 2, L = 223$, $\eta = 4.2$].

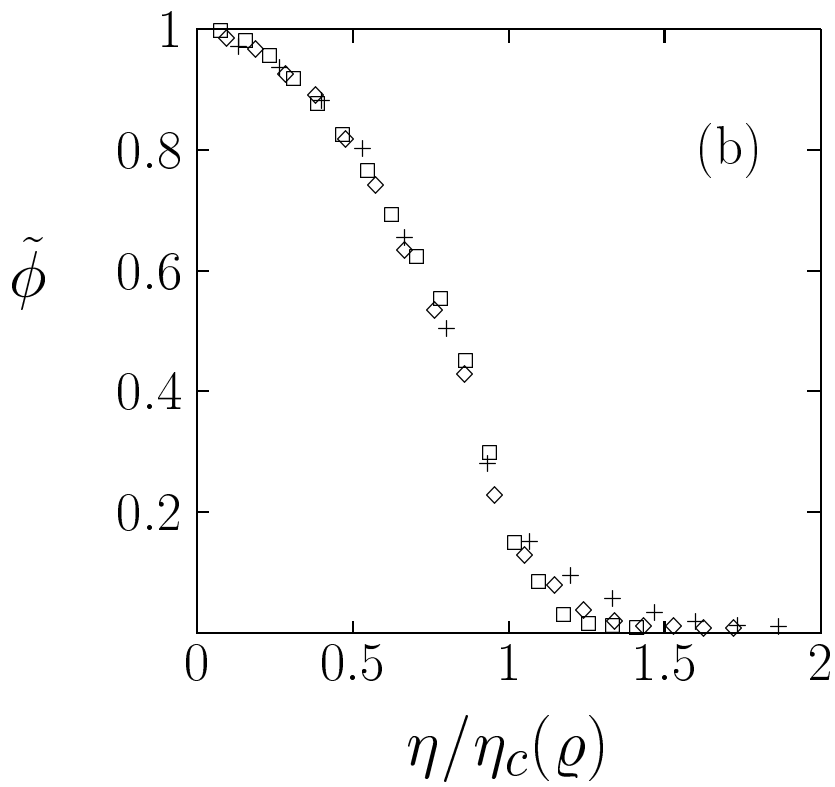
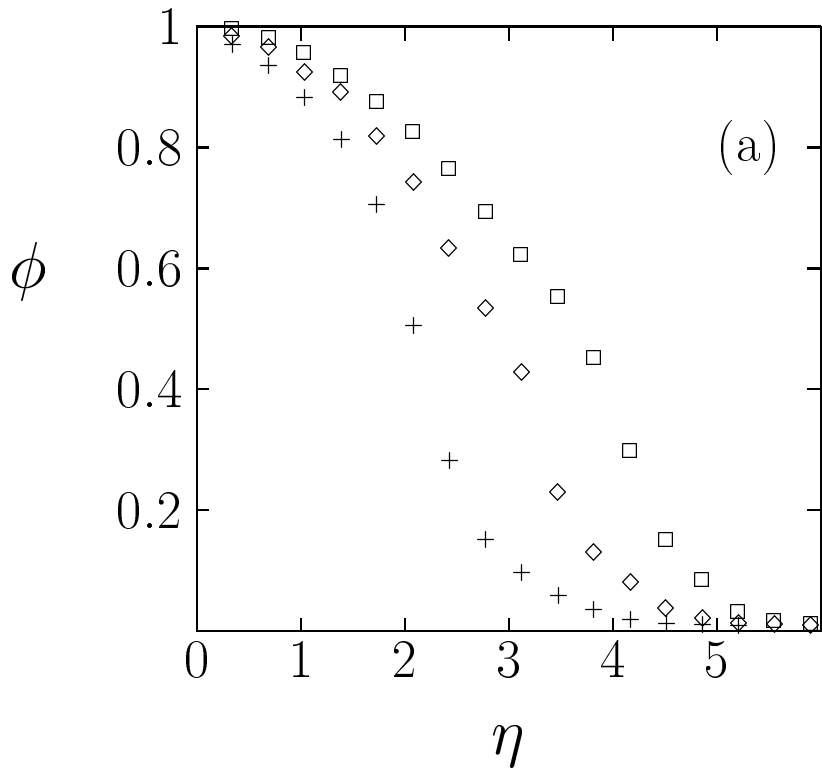
FIG. 8. The susceptibility of the system obtained with two different methods: (\square with error bars) applying definition (15), and (\diamond) from data collapse in the $\phi_{\text{sat}} > \phi > \phi_{\text{noise}}$ regime, which is a more precise procedure for $\eta > \eta_c$. The data suggest that in this case the divergence is *asymmetric*: $\gamma'_* \approx 1$ (solid line) and $\gamma_* \approx 4$ (dotted line).

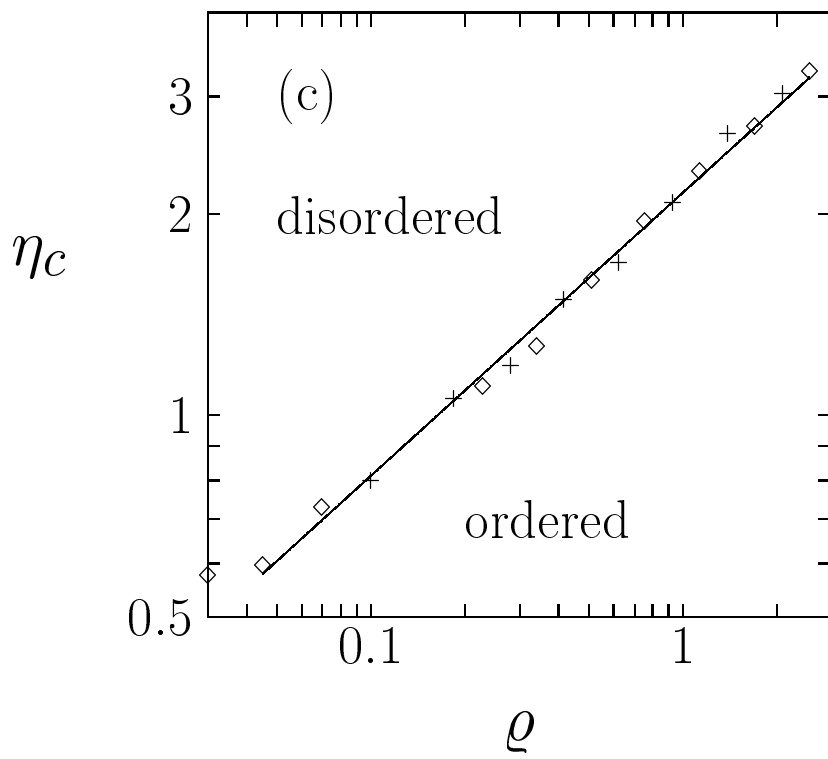
FIG. 9. Snapshots of the time development of a system with $N = 4000$, $L = 40$ and $v_0 = 0.01$ at 50 (a), 100 (b), 400 (c) and 3000 (d) Monte-Carlo steps. First the behavior is reminiscent of the equilibrium XY model, where the long range order is missing since vortices are present in the system. However the vortices are unstable, and finally a self-organized long-range order develops.

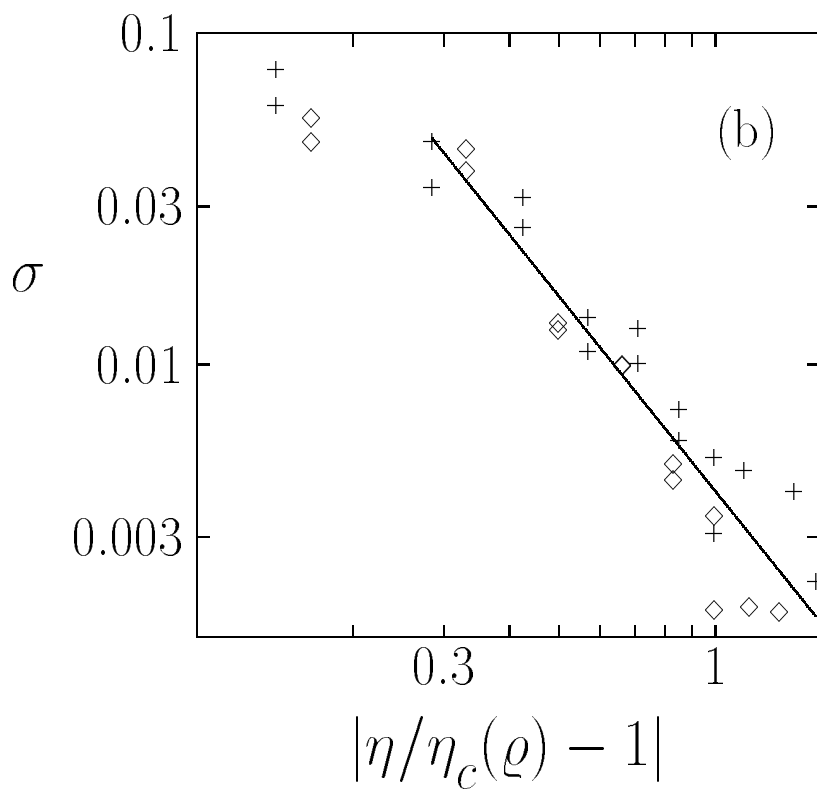
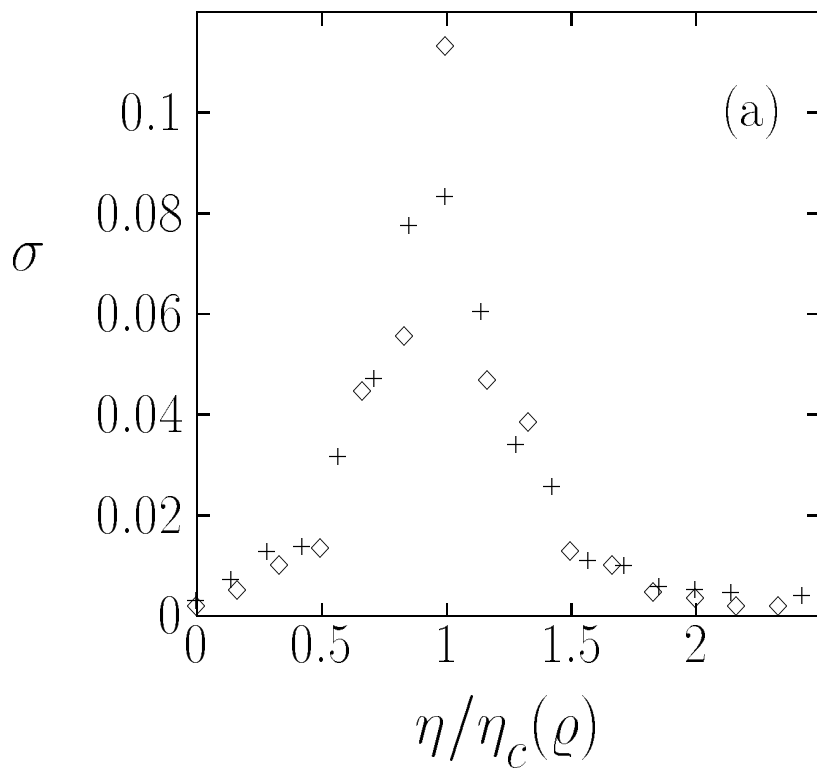


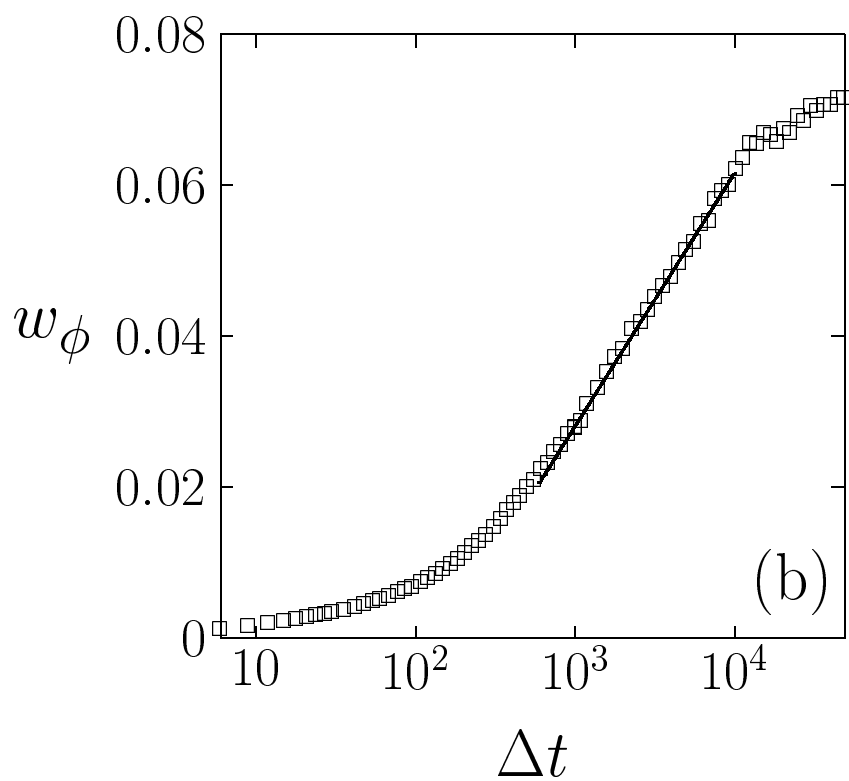
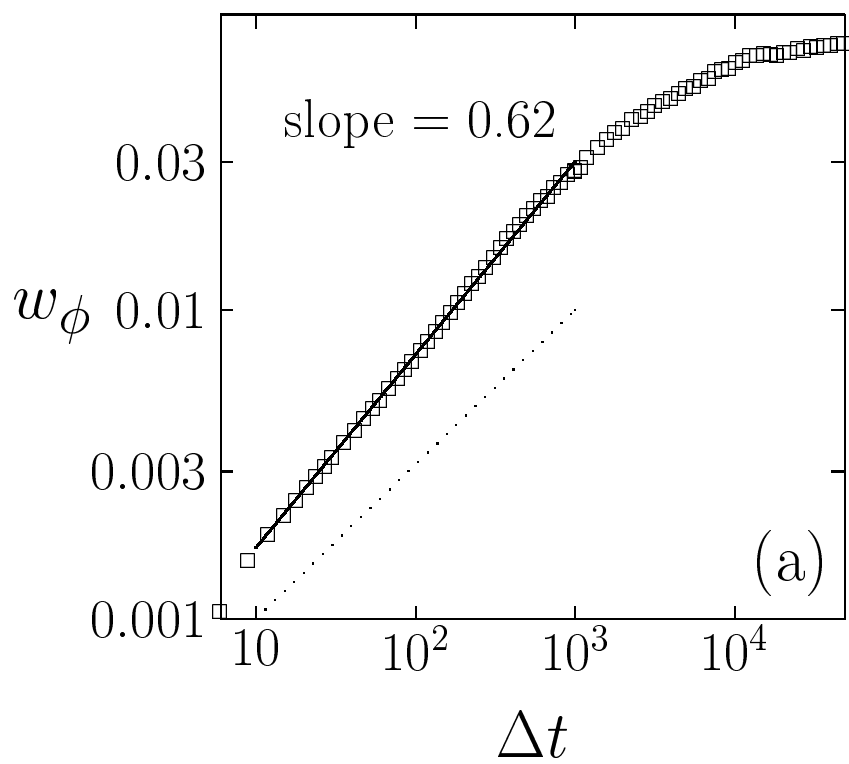












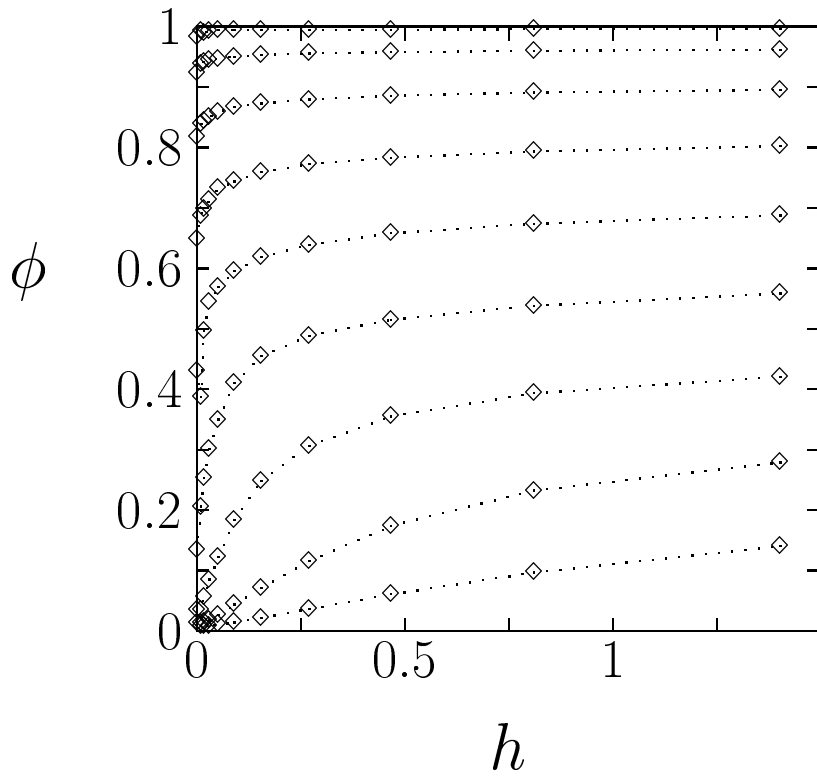
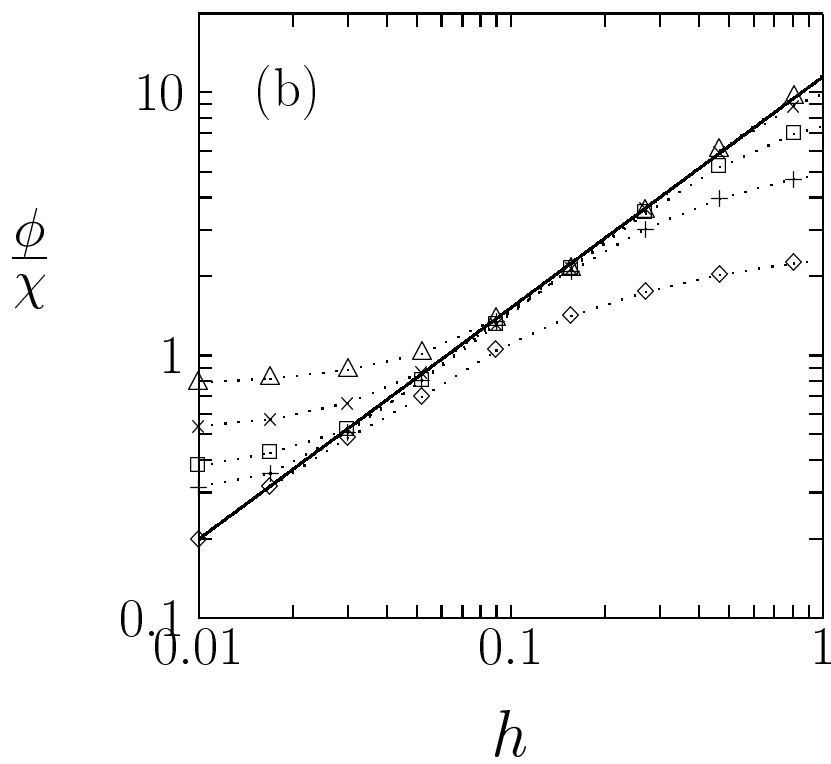
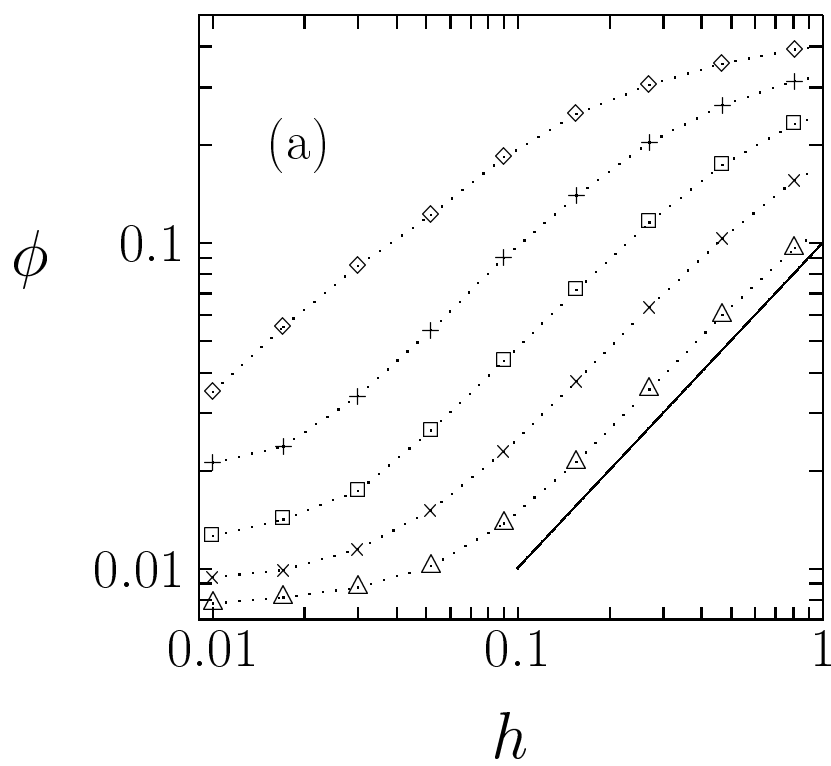


Fig. 6.



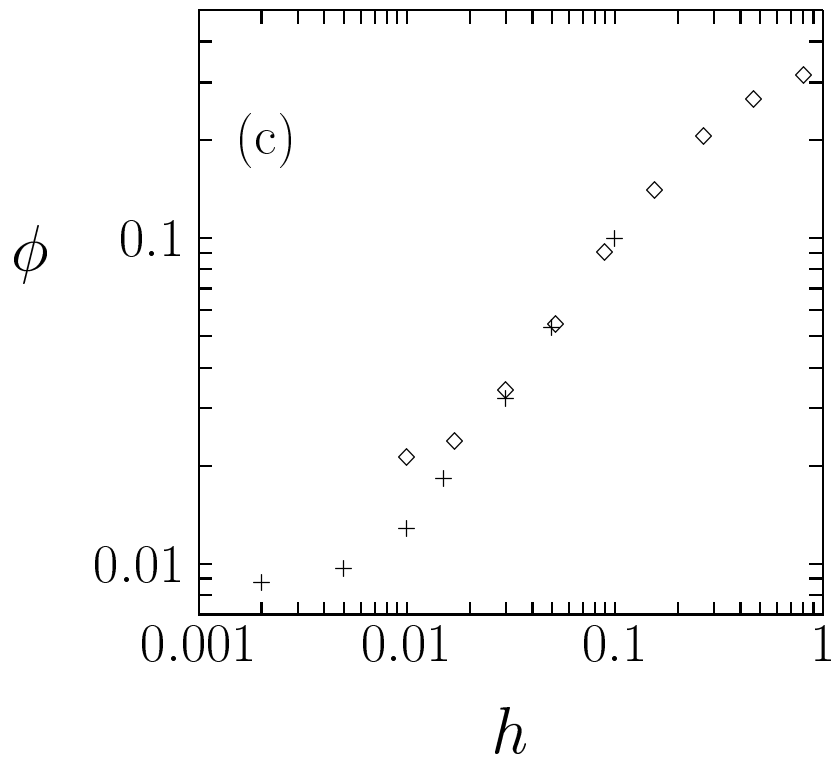


Fig. 7.

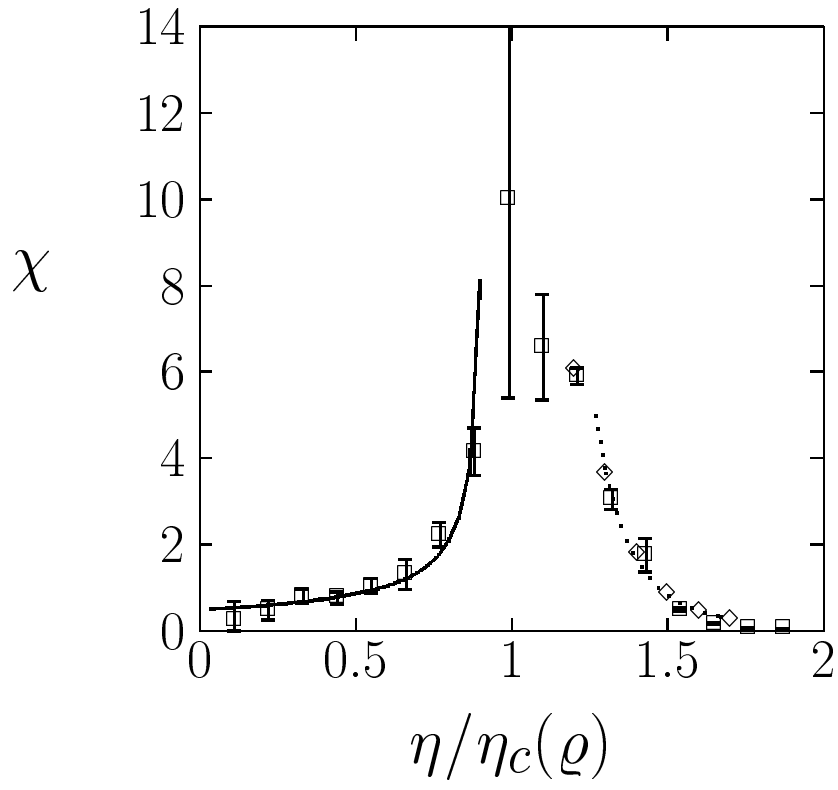


Fig. 8.

